International Journal of Technology
http://ijtech.eng.ui.ac.id

Research Article

Microstructural, Physical, and Mechanical Characteristics of Silver-Modified Tin–Copper–Zinc Lead-Free Solder Alloys

Andromeda Dwi Laksono[1,2*], Gabriel Batistuta Pamurrung[1], Hizkia Alpha Dewanto[1,2], Jatmoko Awali[1], Yee-wen Yen[3], Satoshi Iikubo[4], Gita Novian Hermana[5], Turnad Lenggo Ginta[6], Mavindra Ramadhani[3,7]

[1]Study Program of Materials and Metallurgical Engineering, Institut Teknologi Kalimantan, Soekarno-Hatta Street Km. 15, Karang Joang, Balikpapan, East Kalimantan, 76127, Indonesia

[2]Center for Green Materials Innovation, Institut Teknologi Kalimantan, Soekarno-Hatta Street Km. 15, Karang Joang, Balikpapan, East Kalimantan, 76127, Indonesia

[3]Department of Materials Science and Engineering, National Taiwan University of Science and Technology, Taipei 10672, Taiwan, R.O.C.

[4]Department of Advanced Materials Science and Engineering, Kyushu University, 744 Motooka Nishi-ku, Fukuoka, 819-0395, Japan

[5]Department of Advanced Materials Engineering, Bandung Polytechnic for Manufacturing, Bandung, 40135, West Java, Indonesia

[6]Research Center for Manufacturing Technology of Production Machinery, National Research and Innovation Agency (BRIN), Kota Tangerang Selatan, Banten 15314, Indonesia

[7]Department of Materials and Metallurgical, Institut Teknologi Sepuluh Nopember, Kampus ITS Sukolilo, 60111, Indonesia

*Corresponding author: andromeda@lecturer.itk.ac.id; Tel.: +62542-8530801; Fax: +62542-8530800

Abstract: The rapid increase in hazardous electronic waste (e-waste), particularly from discarded printed circuit boards (PCBs), has become a pressing environmental issue that demands urgent solutions. The development of environmentally friendly solder materials that can replace the conventional Sn–Pb solder, which poses significant health and ecological risks due to its toxic lead content, is one of the critical aspects of addressing this challenge. In this study, a lead-free Sn–0.7Cu–7Zn–xAg alloy (x = 0%, 3%, 3.5%, and 4%) was systematically investigated as a promising candidate for sustainable soldering applications. The alloys were synthesized by melting at 500 °C for 30 min, followed by comprehensive characterization involving density and Vickers hardness testing, Differential Scanning Calorimetry (DSC), and microstructural analysis using SEM-EDS techniques. The results revealed that the addition of 3–4 wt% Ag significantly enhanced the alloy's performance, particularly through the formation of ϵ-$AgZn_3$ phase, which replaced γ-Cu_5Zn_8. This substitution resulted in a narrower melting range, higher melting point, improved wettability, and greater mechanical strength. The highest hardness value of 16.36 Hv was achieved at 4 wt% Ag, primarily due to precipitate strengthening induced by the $AgZn_3$ phase.

Keywords: $AgZn_3$ phase; Lead-free solder; Microstructural analysis; Sn-Cu-Zn-Ag alloy; Vickers hardness

1. Introduction

Due to the rapid growth of electronic device consumption and short product lifecycles, electronic waste (e-waste) has emerged as a critical global issue. Classified as hazardous and toxic, e-waste contains a wide range of metals and chemicals that pose significant risks to both the environment and human health if not properly managed (Ghulam and Abushammala, 2023;

https://doi.org/10.14716/ijtech.v17i2.8271
Received November 2025; Revised December 2025; Accepted January 2026

Sarkar et al., 2022). Printed circuit boards (PCBs), which are integral to nearly all electronic devices, are among the key components contributing to e-waste (Suwandi et al., 2019). PCBs consist of conductive pathways that connect various electronic components and rely on solder materials to ensure electrical conductivity and mechanical stability (Sankar et al., 2022; Kaya, 2019; Ariati et al., 2016).

Conventional solder materials, particularly Sn-Pb alloys, have been widely used due to their low cost and favorable soldering characteristics. Lead (Pb) is a toxic heavy metal known to cause neurological damage and environmental contamination. As a result, there has been increasing pressure from both regulatory bodies and environmental advocates to eliminate the use of Pb in electronics manufacturing (Chen et al., 2021; Perkins et al., 2014; Ganesan and Pecht, 2006). Consequently, researchers have focused on developing Pb-free solder alternatives that deliver comparable or superior performance without the associated toxicity. Among the many proposed lead-free alloys, tin (Sn)-based systems remain the most promising due to their excellent solderability, availability, and compatibility with existing PCB materials, especially copper (Hillman et al., 2018; Y. Zhang, 2011). Copper (Cu), silver (Ag), and zinc (Zn) alloying elements are commonly added to modify the microstructure and enhance the mechanical and thermal properties (Cui et al., 2023; Murugesan et al., 2023). Cu improves mechanical strength and electrical conductivity (Yang et al., 2020), whereas Ag enhances joint strength and thermal fatigue resistance (Hamasha et al., 2023). Zn offers potential benefits in reducing oxidation and improving wettability (Huang et al., 2013).

Recent studies have increasingly focused on optimizing lead-free solder alloys through elemental additions to improve their mechanical and thermal characteristics. Siahaan et al. investigated Sn–0.7Cu–xAg systems and demonstrated that the incorporation of Ag (1–2 wt%) increases the density, melting temperature, hardness, and shear strength of the solder, thereby improving the overall mechanical reliability of the solder (Siahaan and Riza, 2020). Similarly, Jayesh et al. explored the effect of Ag addition in Sn–0.5Cu–3Bi ternary systems and observed that increasing the Ag concentration (up to 1 wt%) enhances both the melting point and microstructural hardness of the alloy (Jayesh and Elias, 2020). Collectively, these studies underscore the critical role of minor alloying elements such as Ag in optimizing the physical and mechanical properties of Sn-based lead-free solder alloys, thereby offering promising alternatives for replacing conventional lead solders in electronic packaging applications.

The ternary and quaternary systems of Sn–Cu–Zn and Sn–Cu–Zn–Ag alloys are currently being investigated to optimize solder properties, including melting behavior, hardness, and microstructural stability. The formation of intermetallic compounds (IMCs) like γ-Cu_5Zn_8 and ϵ-$AgZn_3$ plays a critical role in determining solder performance (Dybeł et al., 2023; Qiu et al., 2021; Gancarz et al., 2018; Mayappan et al., 2011; Lai et al., 2009; Yu et al., 2001). The ϵ-$AgZn_3$ phase, in particular, has been shown to improve mechanical strength and refine grain structure, making Sn-Cu-Zn with Ag addition a promising candidate for the development of lead-free solders. In comparison to binary Sn–Zn solders, research on Sn–Zn–Cu ternary solders (such as Sn-9Zn-2Cu) has examined the microstructure, mechanical characteristics, and tensile behavior, demonstrating that the addition of Cu enhances strength and wettability by modifying IMC formation and refining microstructure (Qiu et al., 2021). Reviews of Sn–Cu-based solders also emphasize the role of alloying elements in tailoring microstructures and improving mechanical performance (Zhao et al., 2019). The design of lead-free solder requires the simultaneous optimization of cost, mechanical dependability, thermal fatigue resistance, and melting range. While predictions in quaternary Sn-Ag-Cu-Zn alloys were shown for different Zn contents, Sn, Ag, and Cu activities in ternary SAC alloys showed negative deviations from ideality at certain compositions, offering a more complete thermodynamic description of these multicomponent systems (You et al., 2021). Although full optimization frameworks are less developed in the literature, multi-element systems, such as Sn–Cu–Zn–Ag, allow customization across various properties. Ag was selected as an alloying addition because trace Ag is widely used in commercial Sn–Ag–Cu lead-free solders — such as SAC305, which contains approximately 3–4 wt%

Ag (Siahaan and Riza, 2020). Previous studies have shown that the addition of small amounts of Ag to Sn–Cu and Sn–Zn solder alloys can significantly reduce the melting temperature and enhance mechanical properties through microstructural refinement and the formation of modified intermetallic compounds (Alam et al., 2015). Therefore, the range of Ag contents from 0 to 4 wt% was adopted to systematically investigate the incremental effects of Ag on melting behavior, hardness, wettability, and microstructure, with 0 wt% Ag serving as the baseline and the upper limit corresponding to the typical industrial range for SAC-type solders. This study investigates the effect of Ag addition (0–4 wt%) on the mechanical and physical properties of Sn–0.7Cu–7Zn solder. The objective of this study is to identify an optimal composition that offers improved hardness, melting characteristics, and microstructural uniformity, thus supporting the development of high-performance, environmentally friendly solder alloys.

2. Materials and Methods

In this study, the preparation of the alloys and the analysis of their microstructural, thermal, and physical properties, including density and wettability, were investigated. Electrical conductivity and fatigue performance were not evaluated at this stage; however, they will be the primary focus of subsequent research phases because these properties are critical to the long-term reliability of solder joints.

2.1 Preparation of the alloys

This study focuses on the development and characterization of lead-free solder alloys based on Sn-0.7Cu-7Zn with the addition of varying amounts of Ag (0%, 3%, 3.5%, and 4%). Raw materials consisting of Sn–0.7Cu (≥99.9%, Logam Makmur, Jakarta, Indonesia), Zn (≥99.9%, Logam Makmur, Jakarta, Indonesia), and Ag (≥99.9%, Logam Makmur, Jakarta, Indonesia) were cut and accurately weighed to obtain a total mass of 50 g. Table 1 presents the detailed mass distribution for each element. The materials were then cleaned by immersion in acetone (Analytic grade ≥99.5%, Kimia Samarinda, Samarinda, Indonesia) for 5 min, HCl (Kimia Samarinda, Samarinda, Indonesia) for 1 min, and alcohol (Kimia Samarinda, Samarinda, Indonesia) for 5 min. The cleaned materials were melted in graphite crucibles using a muffle furnace set at 500°C for 30 min. The resulting molten solder was cast into graphite molds and allowed to cool to room temperature. The experimental setup is depicted in the schematic in Figure 1.

Table 1 Mass balance for each alloy composition

Alloy	Total mass (g)	Zn (wt.%)	Ag (wt.%)	Sn-0.7Cu (wt.%)
Sn-0.7Cu-7Zn	50.0	3.5	-	46.5
Sn-0.7Cu-7Zn-3Ag	50.0	3.5	1.5	45.0
Sn-0.7Cu-7Zn-3.5Ag	50.0	3.5	1.75	44.75
Sn-0.7Cu-7Zn-4Ag	50.0	3.5	2.0	44.5

2.2 Microstructural Characterization

Microstructural characterization was conducted using scanning electron microscopy-energy dispersive X-ray spectroscopy (SEM-EDS; Phenom ProX, Thermo Fisher Scientific, Waltham, MA, USA). Prior to analysis, the specimens were ground using abrasive papers and mounted onto holders. SEM-EDS examinations were conducted using a Phenom World instrument at a magnification of 5000, enabling detailed observations of surface morphology and elemental composition. The resulting micrographs and compositional data were used to evaluate the uniformity and phase distribution of the solder samples.

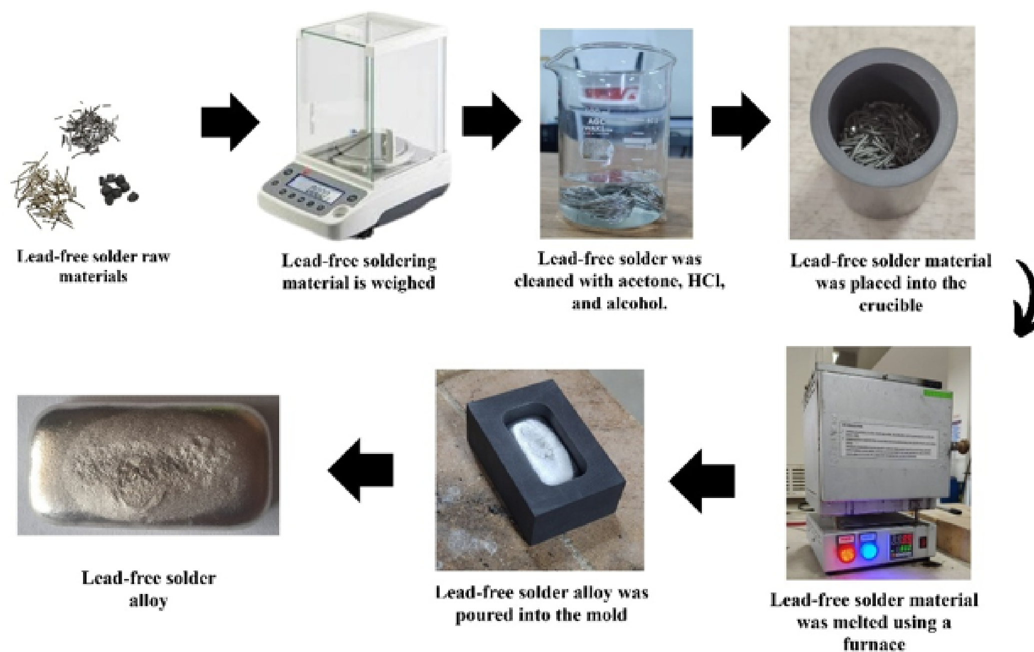

Figure 1 Schematic diagram of alloy fabrication process using a graphite mold

2.3 Thermal Analysis

Thermal analysis was performed using Differential Scanning Calorimetry (DSC; Setaram Instrumentation, Lyon, France) to determine the phase transition behavior and melting characteristics of the solder alloys. Approximately 1 g of each sample was sealed in a crucible and placed alongside a reference into the DSC chamber. The samples were heated from 120°C to 260°C at a rate of 5°C/min. Thermograms were recorded and analyzed to identify onset and peak melting temperatures, which are critical for evaluating solder processability.

2.4 Physical and Mechanical Testing

Mechanical testing included hardness, density, and wettability evaluations. For the Vickers Hardness Tester (FM Series, Future-Tech Corp., Kawasaki, Japan), the surfaces of the samples were polished using a Vickers indenter before applying a 5 N load. Hardness values were computed based on the indentations' size. Density measurements were conducted using Archimedes' principle: a 100 mL scale-marked cylinder was filled with 50 mL of distilled water (Kimia Samarinda, Samarinda, Indonesia), and the mass of each sample was recorded before being submerged. The volume of displaced water was recorded, and the density was calculated accordingly. Wettability testing involved cleaning a copper plate (≥99.9%, Toko Besi & Logam Samarinda, Samarinda, Indonesia) (150 mm × 150 mm) with 10% HCl, placing 1 g of solder onto the hot plate, and heating it at 260°C for 180 s. After cooling, the solder's spread area was analyzed using ImageJ software.

3. Results and Discussion

3.1 Microstructure of the As-Casted Sn–0.7Cu–7Zn–xAg Alloy

Figure 2 shows the phase equilibria and cooling behavior of the Cu–Sn–Zn system calculated using Pandat 2025 Software. The isothermal sections at 200°C (Figure 2a) and 300°C (Figure 2b) display phase stability regions with increased solubility and phase boundary shifts at higher temperatures. The isopleth section at 7 wt.% Zn (Figure 2c) illustrates the phase transformations with increasing Sn content, including the formation of liquid, solid solution, and intermetallic phases. The cooling curve of the Sn–0.7Cu–7Zn alloy (Figure 2d) revealed

multiple thermal arrests, indicating complex solidification behavior typical of multicomponent solder alloys. Although the calculated phase diagrams in Figure 2 are restricted to the ternary Cu–Sn–Zn system and do not explicitly include Ag, they provide an important baseline for interpreting the experimental behavior of the quaternary Sn–0.7Cu–7Zn–xAg alloys. The predicted phase fields and cooling paths clarify how the Sn–0.7Cu–7Zn composition solidifies in the absence of Ag, highlighting the formation of liquid, solid-solution, and intermetallic phases.

The isothermal sections at 200 °C and 300 °C predict that the alloy composition lies within phase fields dominated by β-(Sn) solid solution, γ-Cu_5Zn_8, and Cu6Sn5-type intermetallic compounds, depending on temperature. The 7 wt.%s Zn isopleth further shows suggests the sequential appearance of the (Cu) solid solution, β-Sn, γ-Cu_5Zn_8, and Cu–Sn–Zn ternary intermetallics during cooling. The cooling curve in Figure 2d reveals multiple thermal arrests corresponding to the formation of β-Sn, γ-Cu_5Zn_8, and Cu_6Sn_5, indicating a complex multistep solidification pathway.

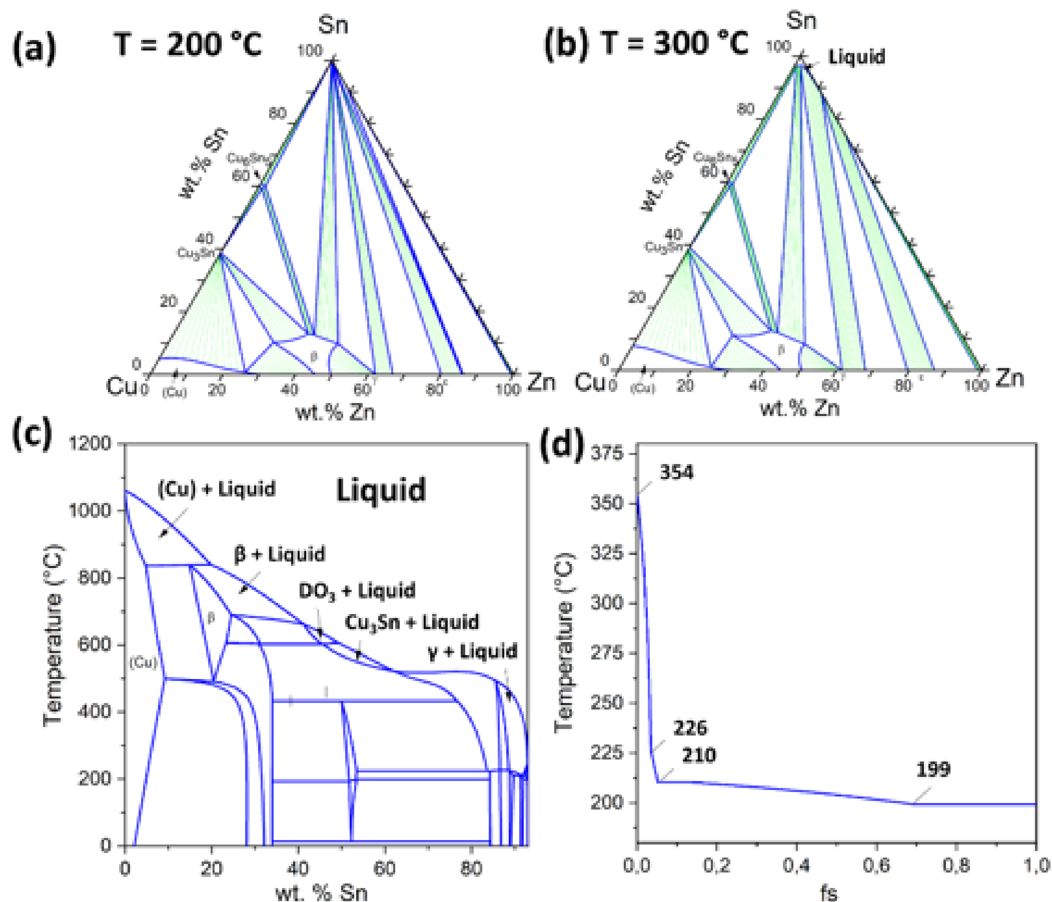

Figure 2 (a) Isothermal section of the Cu–Sn–Zn system at 200°C, (b) Isothermal section of the Cu–Sn–Zn system at 300°C, (c) Isopleth section of the Cu–Sn–Zn system at 7 wt.% Zn, and (d) Cooling curve of the Sn–0.7Cu–7Zn alloy

Figure 3 shows the SEM images in the backscattered electron image (BEI) mode of the Sn-Cu-Zn-Ag solder alloys. The presence of intermetallic compound (IMC) can be observed, exhibiting variations in color, intensity, and size that reflect differences in thickness and morphology among the samples. Figure 3(a), the Sn-0.7Cu-7Zn alloy without Ag addition shows the initial formation of IMCs. However, with the incorporation of Ag, as shown in Figures 3(b), 3(c), and 3(d), both the size and distribution of the IMCs significantly increase. The addition of Ag influences the distribution and size of the IMC, where the microstructure consists of Sn grains (bright phase) and eutectic regions containing IMCs (dark phase). These observations indicate that the area and spread of IMCs increase with higher Ag content, revealing that Ag accelerates elemental diffusion and promotes IMC growth on the solder surface.

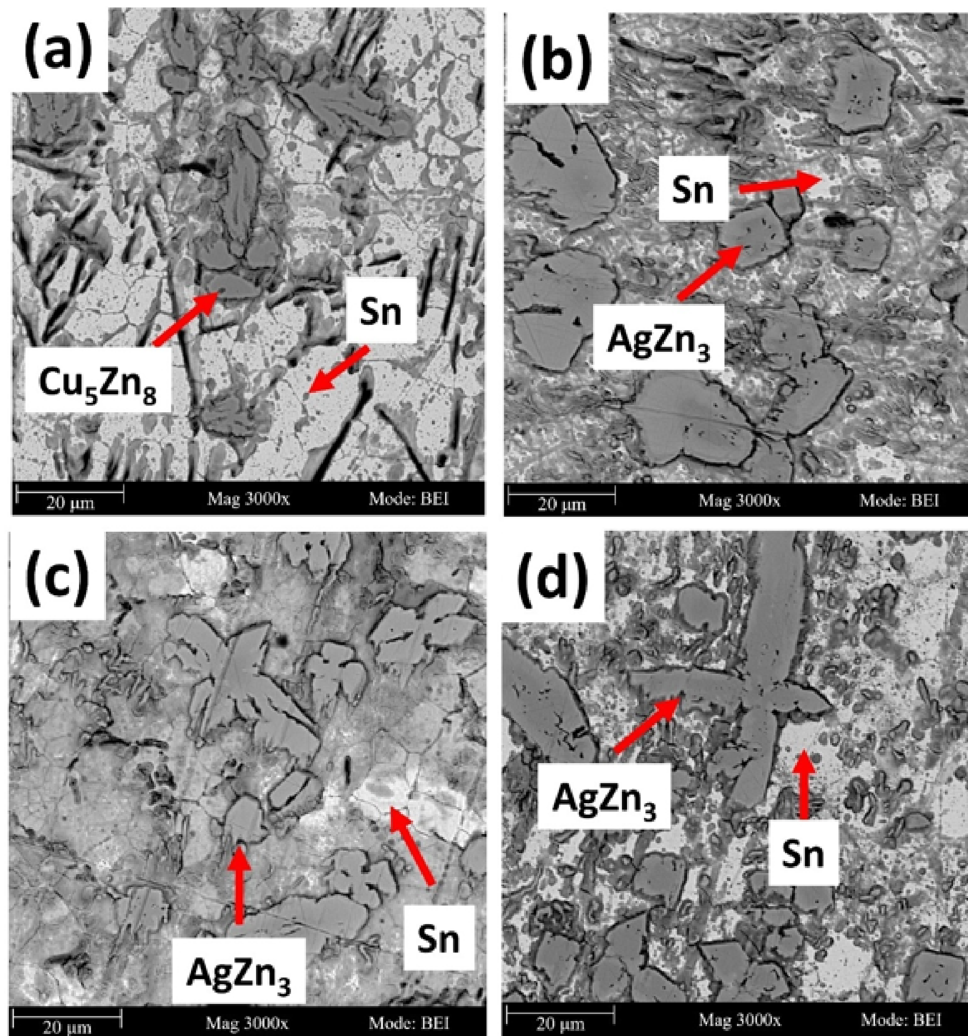

Figure 3 SEM images in backscattered electron (BEI) mode at 3000× magnification of the solder alloys: (a) Sn-0.7Cu-7Zn, (b) Sn-0.7Cu-7Zn-3Ag, (c) Sn-0.7Cu-7Zn-3.5Ag, and (d) Sn-0.7Cu-7Zn-4Ag

Following SEM analysis to observe the surface morphology of the solder samples, Energy Dispersive X-ray Spectroscopy (EDS) was performed on the corresponding areas to determine the elemental composition of the IMCs, especially in regions with differing contrast and size, which are believed to result from varying Ag additions in the alloys. Identifying the constituent elements of the compound allows for the prediction of the types of intermetallic phases formed, providing deeper insight into the role of Ag in the growth of intermetallic compounds in the lead-free Sn-0.7Cu-7Zn solder alloy. The EDS analysis of the Sn–0.7Cu–7Zn solder alloy revealed that the dark-colored IMC features exhibited a shell-like morphology. Elemental analysis of the dark phase (Figure 3(a)) shows a dominant composition of 56.38 at% Zn and 30.10 at% Cu, as shown in Table 2. According to Liu et al. (2020), the Cu_5Zn_8 IMC forms through interaction between Zn and Cu, particularly when Zn is dominant (Liu et al., 2020) at approximately which aligns well with the findings in this study. The presence of Cu_5Zn_8 was further confirmed by empirical calculations based on the work of Gourdon et al., 2007, who reported a composition of 61.39 wt% Zn and 31.86 wt% Cu, resulting in the empirical formula Zn_30Cu_{16} with a Zn:Cu atomic ratio of 1.875 (Gourdon et al., 2007). This closely matches the theoretical ratio of 1.6 for Cu_5Zn_8 formation, which is 1.6, thereby supporting the identification of the IMC phase as Cu_5Zn_8. The growth of the Cu_5Zn_8 phase is driven by the rapid diffusion of Cu atoms into the solder matrix, while Zn atoms diffuse toward the joint interface and control the formation of Cu-Zn compounds.

During the initial stage of soldering, Cu-Zn phases tend to form more readily than Cu-Sn phases due to differences in diffusion rates and Gibbs free energy (Mayappan et al., 2011). EDX analysis of the Sn–0.7Cu–7Zn–3Ag sample (Figure 3(b)), performed on the dark phase, revealed that the composition is predominantly 24.63 at% Ag and 50.82 at% Zn, as shown in Table 2. These values indicate the formation of an ϵ-$AgZn_3$ IMC phase. The presence of this phase is further supported by the findings of Oh et al., 2024, who reported that ϵ-$AgZn_3$ forms within the composition range of 12–24 at% Ag and is characterized by a dark gray appearance and a smooth surface morphology. Meanwhile, the bright phase indicates the dominance of Sn, which results in a lighter appearance in the microstructure. The same phase also appears alongside the increasing formation of $AgZn_3$, which becomes more pronounced at Ag concentrations of 3.5–4 wt.% (Figures 3(c)–(d)). This phenomenon is attributed to the direct interaction between the Ag and Zn atoms during the melting process. The increased Ag content accelerated the formation of the Ag-Zn solid phase, thereby slowing the overall solidification process. Consequently, a longer time is available for the growth of intermetallic compounds, including ϵ-$AgZn_3$ (Song and Lin, 2004). It is evident that $AgZn_3$ grows in the presence of Ag and competes with Cu_5Zn_8 in this study.

Table 2 Elemental composition based on the spot-EDS analysis in Figure 3

Figure	Element symbol	At.%	Wt.%	Prediction phase
3(a)	Zn	56.38	61.39	Cu_5Zn_8
	Cu	30.10	31.86	
	Sn	1.84	3.64	
	O	11.67	3.11	
3(a)	Sn	51.19	88.06	Sn
	O	47.94	11.12	
	Zn	0.88	0.83	
3(b)	Zn	50.82	47.50	$AgZn_3$
	Ag	24.63	37.98	
	Cu	8.40	7.63	
	Sn	2.17	3.69	
3(b)	Sn	58.94	91.42	Sn
	O	41.06	8.58	
3(c)	Zn	49.56	45.91	$AgZn_3$
	Ag	27.83	42.53	
	Cu	4.68	4.21	
	Sn	2.26	3.80	
	O	15.67	3.55	
3(c)	Sn	58.37	91.23	Sn
	O	41.63	8.77	
3(d)	Zn	53.11	47.72	$AgZn_3$
	Ag	25.55	37.87	
	Cu	10.84	9.47	
	Sn	1.86	3.03	
	O	8.64	1.90	
3(d)	Sn	16.09	57.11	Sn
	O	82.06	39.26	

3.2 Thermal Analysis

In this experiment, the samples were heated in a controlled manner within a temperature range of 120°C–260°C, using a constant heating rate of 5°C/min. The heating process was conducted using a Themys One simultaneous thermal analyzer. Table 3 summarizes the phase transition parameters obtained from the Differential Scanning Calorimetry (DSC) analysis. The first transition temperature (T_1) represents the initial structural transformation detected during heating. The onset temperature (T_{onset}) is the point at which melting begins, as identified by the initial deviation in the DSC curve. The liquidus temperature (T_L) represents the temperature at which the entire material is fully in the liquid phase, whereas the end temperature (T_{end}) signifies the completion of the melting process.

Table 3 Phase transition temperatures in the solder alloys

Alloy	T_1 (°C)	T_{onset} (°C)	T_L (°C)	T_{end} (°C)	($T_{\mathrm{end}}-T_{\mathrm{onset}}$) (°C)
Sn-0.7Cu-7Zn	195.90	210.01	215.35	217.92	7.91
Sn-0.7Cu-7Zn-3Ag	194.42	220.21	224.11	227.74	7.53
Sn-0.7Cu-7Zn-3.5Ag	210.01	220.02	225.18	227.11	7.09
Sn-0.7Cu-7Zn-4Ag	214.11	223.87	227.96	232.05	7.08
*SAC305	217	217	231	-	-
*Sn-37Pb	183	183	183	-	-

*Muzni et al., 2023

The DSC results for the Sn-0.7Cu-7Zn alloy with varying Ag additions show that the presence of Ag influences the alloy's thermal behavior (Figure 4). In the Ag-free sample, the melting transition range ($Tend$ – $Tonset$) is relatively wide, at approximately 7.91°C, indicating a less uniform melting process. It is typically attributed to an inhomogeneous microstructure, where individual phases melt at different temperatures, resulting in a gradual rather than a sharp melting transition. However, with the addition of 3%, 3.5%, and 4% Ag, the transition range narrows to 7.53°C, 7.09°C, and 7.08°C, respectively. The narrowing of the melting range suggests that Ag improves the melting process's homogeneity, a desirable thermal characteristic that ensures the solder remains fully liquid only for a short duration during solidification, thereby facilitating high-quality joint formation. Another study reported that a solder with the composition Sn-3.5Ag-0.3Zn exhibits a melting range of 8.34 °C (Muala, 2022), which is wider than that observed in the present study.

In addition, the incorporation of Ag into the Sn-0.7Cu-7Zn alloy significantly increases the liquidus temperature (TL). For the Ag-free alloy, (TL) is recorded at 215.35°C. With the addition of 3%, 3.5%, and 4% Ag, the (TL) increases progressively to 224.11°C, 225.18°C, and 227.96°C, respectively. This increase in the transition temperature indicates that Ag strengthens the atomic bonding within the alloy, requiring higher thermal energy to induce melting. This phenomenon is attributed to the formation of thermally stable Ag-Zn intermetallic phases, as also reported by Czaja et al., 2023 who demonstrated that the presence of Ag in lead-free solder alloys improves thermal stability and strengthens interphase bonding. Enhanced thermal and microstructural stability is crucial for ensuring the long-term reliability of lead-free solder joints in electronic packaging (Jiang et al., 2019).

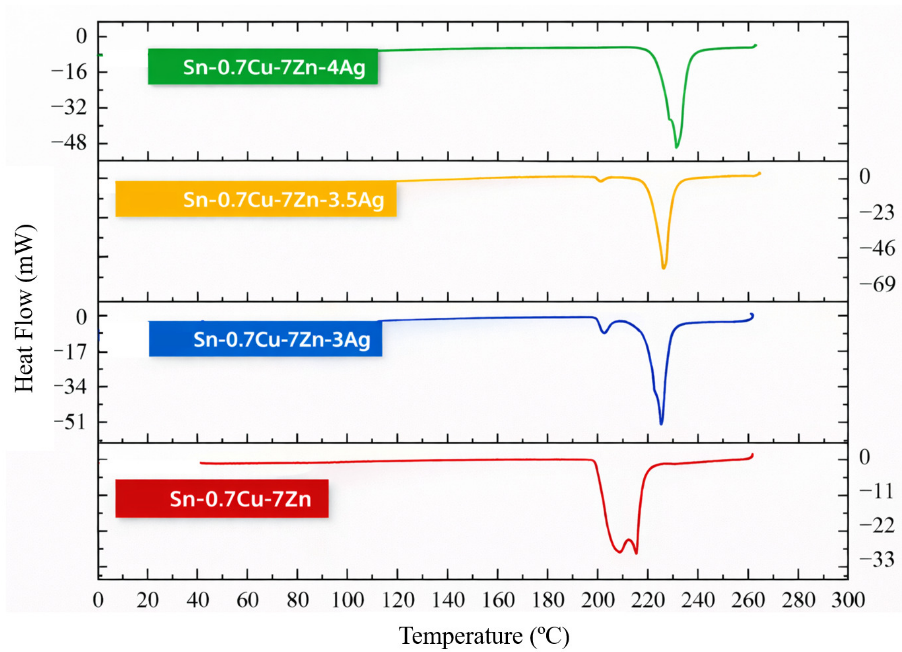

Figure 4 DSC Curve of lead-free Sn-Cu-Zn-Ag solder alloy

3.3 Wettability Analysis

The wettability test aims to evaluate the extent to which the lead-free solder alloy can spread across the surface of a copper substrate. In this test, a copper plate measuring 150 mm × 150 mm was used as the substrate, and 1 gram of lead-free solder alloy was used as the test material. The wetted area was quantitatively measured using ImageJ software. Photographs of the solder spread were captured from a top-view perspective, and the wetted area was subsequently calculated using ImageJ software. These data were used to evaluate solder wettability, which is an important parameter for assessing solder joints' performance and reliability in electronic applications. The solder sample was placed on a copper plate and heated at 260°C for 180 s. After heating, the sample was allowed to cool to room temperature, and the solder's spreading area on the substrate was measured. Measurements were conducted quantitatively using ImageJ software. The obtained data were used to assess the wettability of the solder, which is a key parameter in determining the performance and reliability of solder joints in electronic applications.

Figure 5 presents the wettability test results of the solder alloys. The molten solder appears as a compact droplet, failing to spread uniformly and forming a dome-like shape, indicating poor wetting behavior. This limited spread ability is primarily attributed to the presence of Zn in the alloy, which rapidly forms an oxide layer on the sample surface. This oxide layer hinders the interaction between the solder and the substrate, thereby reducing wettability. The oxidation mechanism was described by Kitajima and Shono, 2005, who explained that oxygen molecules from the air adsorb onto the Zn surface and attract Zn electrons to form a zinc oxide film. Furthermore, additional oxygen molecules may penetrate this oxide layer, promoting further diffusion reactions within the solder and resulting in a thicker oxide layer. As a result, the wettability of the solder in air deteriorates significantly. These findings are supported by Xiao et al., 2023, who reported that when the Zn content exceeds 1.5%, the surface tension of the molten solder increases and Zn oxide formation accelerates, ultimately degrading the overall wettability (Xiao et al., 2023).

Based on the wettability test results in Table 4, the addition of Ag to the Sn-0.7Cu-7Zn alloy has a positive effect on the wetting behavior of the solder. The Ag-free alloy exhibited an average wetting area of 4.61 mm^2, which is relatively low and exhibited considerable variation

among repetitions. The addition of 3% Ag increased the average wetting area to 4.88 mm^2, indicating an improvement in wettability. At 3.5% Ag, the average wetting area reached 5.49 mm^2, while the highest value was recorded at 4% Ag, with a wetting area of 6.69 mm^2 and very consistent results, as evidenced by the reduced standard deviation across repeated tests. The improvement in wetting performance and result consistency shows that Ag plays a crucial role in enhancing the spreading ability of the solder on the substrate. This is likely due to the ability of Ag to lower the surface tension of molten solders and increase its affinity for the metallic surface. These findings are consistent with those of (Xiao et al., 2023) who stated that Ag content in solder alloys significantly influences wettability, while reducing Ag content tends to result in poorer wetting performance.

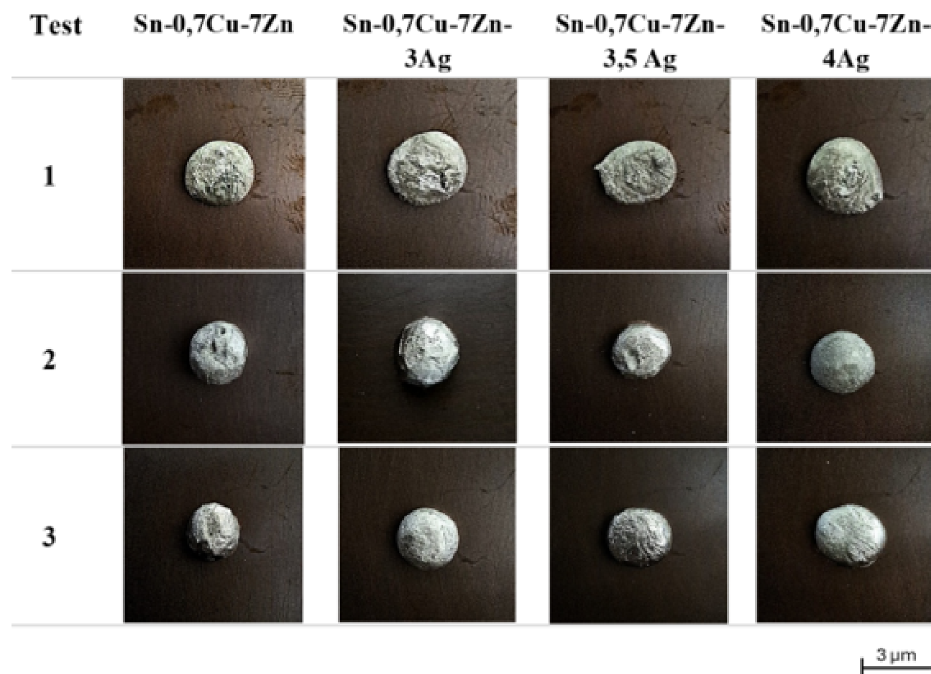

Figure 5 Top view of the wettability test results for the solder alloy on the substrate

Table 4 The area of the solder alloy wettability test results

Alloy	Test (mm^2)			Average (mm^2)	Standard deviation
	1	2	3		
Sn-0.7Cu-7Zn	5.62	4.17	4.05	4.61	0.97
Sn-0.7Cu-7Zn-3Ag	5.90	4.66	4.10	4.88	0.82
Sn-0.7Cu-7Zn-3.5Ag	5.99	5.68	4.82	5.49	0.60
Sn-0.7Cu-7Zn-4Ag	6.43	6.83	6.82	6.69	0.22
*SAC305	-	-	-	5.60	-
*SAC305-0.5TiO_2-0.5Al_2O_3	-	-	-	7.32	-

*Muzni et al., 2023

3.4 Density Analysis

Based on Table 5, the results of the density measurement using the Archimedes method indicate that the gradual addition of Ag to the Sn-0.7Cu-7Zn alloy increases the alloy's density. The density measurements revealed considerable variation, particularly in the Ag-free alloy. The density of Sn-0.7Cu-7Zn without Ag ranged significantly from 4.46 to 6.38 g/cm^3, revealing a

high standard deviation, probably due to inhomogeneities in the internal structure of the alloy. When exposed to heat, Zn is highly prone to oxidation, forming oxide layers that are often not uniformly distributed and insoluble in the metal matrix. These oxide inclusions result in non-uniform mass distribution and promote elemental segregation. As a result, certain areas of the alloy become relatively heavier or lighter than others, which is reflected in the inconsistent density measurements across repeated tests.

Table 5 Density measurement results

Alloy	Test (g/ml)			Average (g/cm^3)	Standard deviation
	1	2	3		
Sn-0.7Cu-7Zn	5.32	6.38	4.46	5.38	0.96
Sn-0.7Cu-7Zn-3Ag	6.70	6.10	6.89	6.56	0.41
Sn-0.7Cu-7Zn-3.5Ag	7.30	7.38	7.60	7.42	0.15
Sn-0.7Cu-7Zn-4Ag	8.04	7.80	8.17	8.00	0.18
*SAC305	-	-	-	7.37	-
*Sn-37Pb	-	-	-	8.60	-

*Muzni et al., 2023

The addition of Ag mitigate the inhomogeneity in the alloy, as observed in the Sn-0.7Cu-7Zn alloys with 3-4% Ag. The inclusion of Ag results in higher and more stable density values compared with the Ag-free alloy. This improvement occurs because Ag is more resistant to oxidation, facilitating a more uniform elemental distribution within the alloy. The increase in density also correlates with the increase in Ag content, given that the density of Ag (10.49 g/cm^3) is significantly higher than that of Sn (7.31 g/cm^3), Cu (8.96 g/cm^3), and Zn (7.14 g/cm^3). Therefore, Ag notably contributes to the overall increase in the density of the alloy. Another finding indicates that Ag modifies the microstructure, whereas the overall composition influences the density and other physical properties (Pu et al., 2023). Furthermore, the increasingly consistent density values at higher Ag contents indicate a more homogeneous microstructure. This observation aligns with the findings of L. L. Zhang et al., 2010, who reported that the addition of Ag enhances the oxidation resistance of Sn-Zn alloys. They also found that Ag can suppress Zn oxidation through the formation of Ag-Zn compounds, which act as a barrier to the reaction between oxygen and Zn.

3.5 Hardness Analysis

The hardness test was performed using a ZwickRoell DuraScan 70 device with a 50-g load and a triangular pyramid-shaped indenter. To ensure accuracy and data consistency, each sample was tested at three different points. The Vickers hardness test results show that the addition of Ag to the Sn–0.7Cu–7Zn alloy significantly enhances the hardness of the material (Table 6). The Ag-free sample exhibited a hardness of 14.43 Hv with a standard deviation of 0.25, indicating a relatively low but stable hardness value. The hardness increased to 14.66 Hv upon the addition of 3% Ag, accompanied by a higher standard deviation of 0.51, demonstrating slight fluctuations between measurements. With 3.5% Ag, the average hardness further increased to 14.76 Hv, and the standard deviation decreased to 0.35, reflecting a more consistent incremental improvement. The most notable increase was observed with the addition of 4% Ag, where the hardness reached 16.36 Hv, although it was accompanied by the highest standard deviation of 1.15.

This sharp increase indicates that at 4% Ag, a greater amount of intermetallic phase precipitation—such as AgZn3—occurs, becoming more dominant in the alloy's microstructure. SEM-EDS observations support these findings, which revealed the presence and distribution of IMC precipitates within the solder alloy. The formation of such precipitates contributes to strengthening through a dispersion hardening mechanism, where intermetallic particles hinder dislocation motion during deformation.

Table 6 Vickers hardness test results of solder alloys

Alloy	Test point (Hv)			Average (Hv)	Standard deviation
	1	2	3		
Sn-0.7Cu-7Zn	14.20	14.70	14.40	14.43	0.25
Sn-0.7Cu-7Zn-3Ag	15.10	14.10	14.80	14.66	0.51
Sn-0.7Cu-7Zn-3.5Ag	14.40	14.80	15.10	14.76	0.35
Sn-0.7Cu-7Zn-4Ag	15.30	17.60	16.20	16.36	1.15
*SAC305	-	-	-	14.10	-
*Sn-37Pb	-	-	-	14.00	-

*Muzni et al., 2023

This observation aligns with the findings of L. L. Zhang et al., 2010 (Teja et al., 2022), who stated that the increased microhardness in lead-free solder alloys can be explained by the classical dispersion strengthening theory. According to this theory, the increase in hardness with Ag addition is attributed to the precipitation strengthening induced by the formation of the $AgZn_3$ intermetallic phase. Fine $AgZn_3$ precipitates act as obstacles to dislocation motion within the Sn-based matrix, thereby increasing plastic deformation resistance. Figure 6 illustrates the role of $AgZn_3$ precipitates in hindering dislocation motion within the Sn-based solder matrix. The observed increase in hardness with increasing Ag content is an expected and favorable outcome. The hardness enhancement observed in this study indicates improved resistance to plastic deformation, which is beneficial for solder joint integrity under mechanical loading.

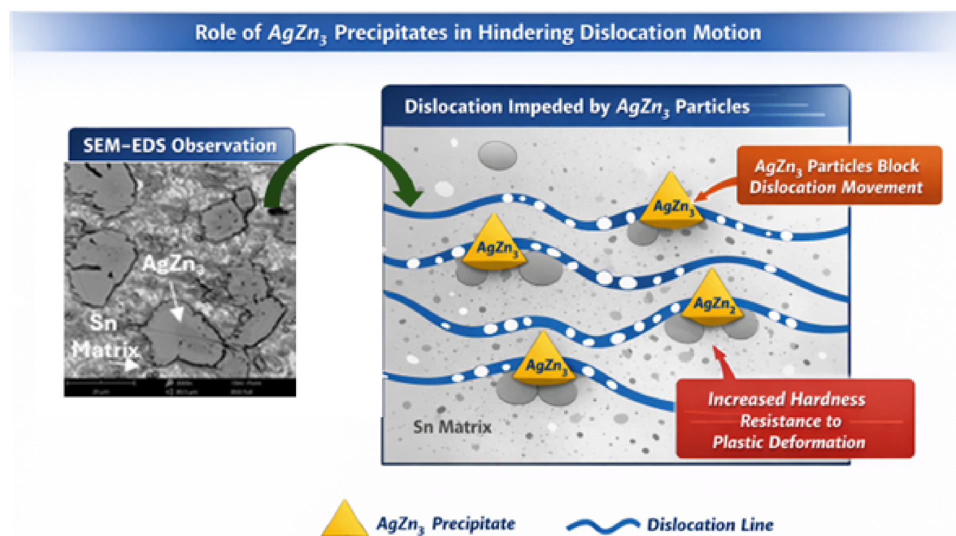

Figure 6 Schematic illustration of $AgZn_3$ precipitates hindering dislocation motion in the Sn-based solder matrix

4. Conclusions

This study demonstrates that the addition of 3%, 3.5%, and 4% Ag to the Sn–0.7Cu–7Zn lead-free solder alloy significantly enhances its physical and mechanical properties, including intermetallic phase formation, thermal characteristics, wettability, density, and hardness. In the absence of Ag, the Cu_5Zn_8 phase is predominantly formed; however, with the incorporation of Ag, a transformation occurs toward the $AgZn_3$ phase, which becomes increasingly dominant with higher Ag content. This phase transformation is accompanied by a narrowing of the melting transition range from 7.91°C to 7.08°C and an increase in the melting point from 215.35°C to 227.96°C, indicating a more homogeneous melting process. Additionally, the solder spread

area increased from 4.61 mm2 to 6.69 mm^2, reflecting improved wettability. The presence of Ag also contributes to higher and more stable density values due to its high atomic mass and oxidation resistance, leading to more uniform elemental distribution. The Vickers hardness test revealed a consistent improvement in hardness with increasing Ag content, with the most notable enhancement observed at 4% Ag, yielding a hardness value of 16.36 Hv. This increase is attributed to the formation of $AgZn_3$ intermetallic precipitates, which strengthen the solder alloy through microstructural reinforcement mechanisms.

Acknowledgements

The authors acknowledge the financial support from the Lembaga Penelitian dan Pengabdian Kepada Masyarakat Institut Teknologi Kalimantan, Indonesia (Grant no. 13288/IT10.L1/PPM.04/2025).

Author Contributions

A.D.L.: conceptualization, methodology, formal analysis, resources, data curation, writing – original draft preparation, writing – review & editing, validation, visualization, supervision, project administration, funding acquisition. G.B.P.: methodology, formal analysis, data curation, investigation, visualization. H.A.D.: writing – review & editing. J.A.: writing – review & editing. Y.W.Y.: methodology, writing – review & editing. S.I.: methodology, writing – review & editing. G.N.H.: writing – review & editing, data curation. T.L.G.: writing – review & editing. M.R.: writing – review & editing.

Conflict of Interest

We have also declared the following: (1). The article is original. (2). The article has been written by the stated authors who are ALL aware of its content and approve its submission. (3). The article has not been published previously. (4). The article is not under consideration for publication elsewhere. (5). No conflict of interest exists, or if such conflict exists, the exact nature must be declared. (6). If accepted, the article will not be published elsewhere in the same form, in any language, without the written consent of the publisher.

References

Alam, S. N., Mishra, P., & Kumar, R. (2015). Effect of ag on sn–cu and sn–zn lead free solders. *Materials Science–Poland*, *33*(2), 317–330. https://doi.org/10.1515/msp-2015-0048

Ariati, M., Nurjaya, D. M., & Rooscote, D. (2016). The effect of double shot peening and nitriding on the die soldering behaviour of h13 and cr-mo-v tool steel. *International Journal of Technology*, *7*(3), 291–319. https://doi.org/10.14716/ijtech.v7i3.2964

Chen, Y., Meng, Z.-C., Gao, L.-Y., & Liu, Z.-Q. (2021). Effect of bi addition on the shear strength and failure mechanism of low-ag lead-free solder joints. *Journal of Materials Science: Materials in Electronics*, *32*, 2172–2186. https://doi.org/10.1007/s10854-020-04982-4

Cui, Y., Xian, J., Zois, A., Marquardt, K., Yasuda, H., & Gourlay, C. (2023). Nucleation and growth of ag3sn in sn-ag and sn-ag-cu solder alloys. *Acta Materialia*, *249*, 118831. https://doi.org/10.1016/j.actamat.2023.118831

Czaja, P., Dybeł, A., & Pstruś, J. (2023). Phase evolution at the interface between liquid solder sn-zn-ag and cu substrate studied by in situ heating scanning transmission electron microscopy. *Journal of Materials Engineering and Performance*, *32*(13), 5749–5755. https://doi.org/10.1007/s11665-023-08284-8

Dybeł, A., Czaja, P., Sitek, J., & Pstruś, J. (2023). Wetting and interfacial chemistry of new pb-free sn-zn-ag-al-li (szaal) solder with cu, ni, and al substrates. *Journal of Materials*

Engineering and Performance, *32*(13), 5723–5730. https://doi.org/10.1007/s11665-023-08155-2

Gancarz, T., Pstruś, J., & Berent, K. (2018). Interfacial reactions of sn–zn–ag–cu alloy on soldered al/cu and al/al joints. *Science and Technology of Welding and Joining*, *23*(7), 558–567. https://doi.org/10.1080/13621718.2018.1427836

Ganesan, S., & Pecht, M. G. (2006). *Lead-free electronics*. John Wiley & Sons.

Ghulam, S. T., & Abushammala, H. (2023). Challenges and opportunities in the management of electronic waste and its impact on human health and environment. *Sustainability*, *15*(3), 1837–1848. https://doi.org/10.3390/su15031837

Gourdon, O., Gout, D., Williams, D. J., Proffen, T., Hobbs, S., & Miller, G. J. (2007). Atomic distributions in the γ-brass structure of the cu–zn system: A structural and theoretical study. *Inorganic Chemistry*, *46*(1), 251–260. https://doi.org/10.1021/ic0616380

Hamasha, M. M., Hamasha, K., & Hamasha, S. D. (2023). Impact of isothermal aging on mechanical properties of 92.8% sn–3%ag–0.5%cu–3.3%bi solder joints. *Metals*, *13*(3), 591. https://doi.org/10.3390/met13030591

Hillman, D., Wilcoxon, R., Pearson, T., McKenna, P., & Collins, R. (2018). Dissolution rate of specific elements in sac305 solder. *Proceedings of SMTA International*, 14–18. https://doi.org/10.37665/smFFXBX73728

Huang, H.-Z., Wang, X.-Q., Tan, D.-Q., & Zhou, L. (2013). Effects of phosphorus addition on the properties of sn-9zn lead-free solder alloy. *International Journal of Minerals, Metallurgy, and Materials*, *20*, 563–567. https://doi.org/10.1007/s12613-013-0766-8

Jayesh, S., & Elias, J. (2020). Experimental investigation on effect of ag addition on sn–0.5cu–3bi. *Metals and Materials International*, *26*, 107–114. https://doi.org/10.1007/s12540-019-00305-3

Jiang, N., Zhang, L., Liu, Z.-Q., Sun, L., Long, W.-M., He, P., Xiong, M.-Y., & Zhao, M. (2019). Reliability issues of lead-free solder joints in electronic devices. *Science and Technology of Advanced Materials*, *20*(1), 876–901. https://doi.org/10.1080/14686996.2019.1640072

Kaya, M. (2019). Printed circuit boards (pcbs). In M. Kaya (Ed.), *Electronic waste and printed circuit board recycling technologies* (pp. 33–57). Springer.

Kitajima, M., & Shono, T. (2005). Development of sn-zn-al lead-free solder alloys. *Fujitsu Scientific and Technical Journal*, *41*(2), 225–235.

Lai, R. S., Lin, K. L., & Salam, B. (2009). Suppressing growth of cu5zn8 layer in sn-zn-ag-al-ga/cu joints. *Journal of Electronic Materials*, *38*(1), 88–92. https://doi.org/10.1007/s11664-008-0579-0

Liu, K., Ding, W., Tao, X., Chen, H., Ouyang, Y., & Du, Y. (2020). Diffusional behaviors and mechanical properties of cu–zn system. *Journal of Alloys and Compounds*, *812*, 152141. https://doi.org/10.1016/j.jallcom.2019.152141

Mayappan, R., Zaman, R. A., Abidin, Z. Z., Asmawati, F. N., & Derman, M. N. (2011). Growth of cu-zn5 and cu5zn8 intermetallic compounds in the sn-9zn/cu joint during liquid state aging. *Advanced Materials Research*, *173*, 90–95. https://doi.org/10.4028/www.scientific.net/AMR.173.90

Muala, A. (2022). Effect of zn addition on alloy by 0.3, 0.6 and 0.9 wt.% on thermal properties, electrical conductivity and microstructure of eutectic sn-3.5ag alloy. *An-Najah Univ Journal A*, *36*(1), 133–156. https://doi.org/10.35552/anujr.a.36.1.2007

Murugesan, R., Venkataramana, S. H., Marimuthu, S., Anand, P. B., Nagaraja, S., Isaac, J. S., Sudharsan, R. R., Khan, T. Y., Almakayeel, N., Islam, S., & Razak, A. (2023). Influence of alloying materials al, cu, and ca on microstructures, mechanical properties, and corrosion resistance of mg alloys for industrial applications: A review. *ACS Omega*, *8*(41), 37641–37653. https://doi.org/10.1021/acsomega.3c03417

Muzni, N. H. M., Mhd Noor, E. E., & Mohd Mustafa Al Bakri Abdullah, M. M. A. B. (2023). Wettability of sn-3.0ag-0.5cu solder reinforced with tio2 and al2o3 nanoparticles at different reflow times. *Nanomaterials*, *13*, 2811. https://doi.org/10.3390/nano13202811

Oh, M., Sakaguchi, H., Kobayashi, E., & Kajihara, M. (2024). Understanding intermetallic compound growth at ag/zn interfaces: Kinetics and mechanisms. *Intermetallics*, *172*, 108378. https://doi.org/10.1016/j.intermet.2024.108378

Perkins, D. N., Brune Drisse, M.-N., Nxele, T., & Sly, P. D. (2014). E-waste: A global hazard. *Annals of Global Health*, *80*(4), 286–295. https://doi.org/10.1016/j.aogh.2014.10.001

Pu, C., Li, C., Dong, T., Miao, Y., Gao, P., Zhang, X., Peng, J., & Yi, J. (2023). Effect of ag addition on the microstructure and corrosion properties of sn–9zn lead-free solder. *Journal of Materials Research and Technology*, *27*, 6400–6411. https://doi.org/10.1016/j.jmrt.2023.11.123

Qiu, J., Peng, Y., Gao, P., & Li, C. (2021). Effect of cu content on performance of sn-zn-cu lead-free solder alloys designed by cluster-plus-glue-atom model. *Materials*, *14*, 2335. https://doi.org/10.3390/ma14092335

Sankar, V. U., Lakshmi, G., & Sankar, Y. S. (2022). A review of various defects in pcb. *Journal of Electronic Testing*, *38*(5), 481–491. https://doi.org/10.1007/s10836-022-06026-7

Sarkar, O., Dey, K. K., Islam, S., & Chattopadhyay, A. (2022). Lead and aquatic ecosystems, biomarkers, and implications for humankind. In *Biomarkers in toxicology* (pp. 1–28). Springer.

Siahaan, E., & Riza, A. (2020). The influences of silver content in lead-free solder sn-0.7cuxag (sac) in physical and mechanical properties. *IOP Conference Series: Materials Science and Engineering*, *1007*, 012025. https://doi.org/10.1088/1757-899X/1007/1/012025

Song, J.-M., & Lin, K.-L. (2004). Double peritectic behavior of ag–zn intermetallics in sn-zn-ag solder alloys. *Journal of Materials Research*, *19*(9), 2719–2724. https://doi.org/10.1557/JMR.2004.0356

Suwandi, D., Aziz, R., Sifa, A., Haris, E., Istiyanto, J., & Whulanza, Y. (2019). Dry film photoresist application to a printed circuit board (pcb) using a maskless photolithography method. *International Journal of Technology*, *10*(5), 1033–1041. https://doi.org/10.14716/ijtech.v10i5.518

Teja, M. B. K., Sharma, A., Das, S., & Das, K. (2022). A review on nanodispersed lead-free solders in electronics: Synthesis, microstructure and intermetallic growth characteristics. *Journal of Materials Science*, *57*(19), 8597–8633. https://doi.org/10.1007/s10853-022-07187-8

Xiao, J., Tong, X., Liang, J., Chen, Q., & Tang, Q. (2023). Microstructure and morphology of the soldering interface of sn–2.0ag–1.5zn low ag content lead-free solder ball and different substrates. *Heliyon*, *9*, e12952. https://doi.org/10.1016/j.heliyon.2023.e12952

Yang, H. Y., Ma, Z. C., Lei, C. H., Meng, L., Fang, Y. T., Liu, J. B., & Wang, H. T. (2020). High strength and high conductivity cu alloys: A review. *Science China Technological Sciences*, *63*, 2505–2517. https://doi.org/10.1007/s11431-020-1633-8

You, Y., Kong, L., Xu, J., Xu, B., Liu, G., & Yang, B. (2021). Prediction of activities of all components in sn-ag-cu and sn-ag-cu-zn lead-free solders using modified molecular interaction volume model. *Results in Chemistry*, *3*, 100143. https://doi.org/10.1016/j.rechem.2021.100143

Yu, S.-P., Wang, M.-C., & Hon, M.-H. (2001). Formation of imcs at eutectic sn–zn–al solder/cu interface. *Journal of Materials Research*, *16*(1), 76–82. https://doi.org/10.1557/JMR.2001.0015

Zhang, L. L., Xue, S. B., Gao, L. L., Sheng, Z., Ye, H., Xiao, Z. X., Zeng, G., Chen, Y., & Yu, S. L. (2010). Development of sn–zn lead-free solders bearing alloying elements. *Journal of Materials Science: Materials in Electronics*, *21*, 1–15. https://doi.org/10.1007/s10854-009-0014-1

Zhang, Y. (2011). Tin and tin alloys for lead-free solder. *Modern Electroplating*, *139*, 204.

Zhao, M., Zhang, L., Liu, Z.-Q., Xiong, M.-Y., & Sun, L. (2019). Structure and properties of sn-cu lead-free solders in electronics packaging. *Science and Technology of Advanced Materials*, *20*(1), 421–444. https://doi.org/10.1080/14686996.2019.1591168